

Available online at [www.sciencedirect.com](http://www.sciencedirect.com)

ScienceDirect

journal homepage: [www.elsevier.com/locate/AJPS](http://www.elsevier.com/locate/AJPS)

## Research Article

# Synergistic chemotherapy/PTT/oxygen enrichment by multifunctional liposomal polydopamine nanoparticles for rheumatoid arthritis treatment

Xiaoling Fu<sup>a,b</sup>, Yutong Song<sup>c</sup>, Xianquan Feng<sup>b</sup>, Zhihong Liu<sup>b</sup>, Wenhao Gao<sup>a,b</sup>, Hongtao Song<sup>a,b,\*</sup>, Qian Zhang<sup>a,\*</sup>

<sup>a</sup>School of Pharmacy, Fujian Medical University, Fuzhou 350108, China

<sup>b</sup>Fuzong Clinical Medical College of Fujian Medical University, Fuzhou 350025, China

<sup>c</sup>First school of clinical medicine, Nanjing Medical University, Nanjing 211166, China

## ARTICLE INFO

## Article history:

Received 14 August 2023

Revised 20 December 2023

Accepted 25 December 2023

Available online 5 February 2024

## Keywords:

Polydopamine

Thermosensitive liposomes

Photothermal therapy

Oxygen generation

Rheumatoid arthritis

## ABSTRACT

Amultifunctional liposomal polydopamine nanoparticle (MPM@Lipo) was designed in this study, to combine chemotherapy, photothermal therapy (PTT) and oxygen enrichment to clear hyperproliferating inflammatory cells and improve the hypoxic microenvironment for rheumatoid arthritis (RA) treatment. MPM@Lipo significantly scavenged intracellular reactive oxygen species and relieved joint hypoxia, thus contributing to the repolarization of M1 macrophages into M2 phenotype. Furthermore, MPM@Lipo could accumulate at inflammatory joints, inhibit the production of inflammatory factors, and protect cartilage *in vivo*, effectively alleviating RA progression in a rat adjuvant-induced arthritis model. Moreover, upon laser irradiation, MPM@Lipo can elevate the temperature to not only significantly obliterate excessively proliferating inflammatory cells but also accelerate the production of methotrexate and oxygen, resulting in excellent RA treatment effects. Overall, the use of synergistic chemotherapy/PTT/oxygen enrichment therapy to treat RA is a powerful potential strategy.

© 2024 Shenyang Pharmaceutical University. Published by Elsevier B.V.

This is an open access article under the CC BY-NC-ND license

(<http://creativecommons.org/licenses/by-nc-nd/4.0/>)

## 1. Introduction

Rheumatoid arthritis (RA) is an autoimmune disease characterized by chronic inflammation, synovial tissue hyperplasia and hypoxia. Inappropriate attack on the joints by the immune system results in a flood of inflammatory

cells infiltrating the joint cavity, which leads to progressive destruction of joint cartilage and eventually disability [1–3]. Methotrexate (MTX) is a commonly used anti-rheumatoid arthritis drug and an anchor drug for RA treatment. However, long-term and high-dose usage of MTX may cause vomiting, hepatotoxicity and bone marrow suppression. Its application has been severely limited due to severe drug resistance and

\* Corresponding authors.

E-mail addresses: [sohoto@vip.163.com](mailto:sohoto@vip.163.com) (H. Song), [1009467948@qq.com](mailto:1009467948@qq.com) (Q. Zhang).

Peer review under responsibility of Shenyang Pharmaceutical University.

<https://doi.org/10.1016/j.ajps.2024.100885>

1818-0876/© 2024 Shenyang Pharmaceutical University. Published by Elsevier B.V. This is an open access article under the CC BY-NC-ND license (<http://creativecommons.org/licenses/by-nc-nd/4.0/>)

adverse reactions [4,5]. Therefore, it is essential to exploit a suitable nanomedicine-based therapeutic strategy to improve the efficacy of RA treatment and reduce the toxicity of MTX by controlling drug release.

Vascular abnormalities and inflammatory cell infiltration in the joint cavity significantly increased vascular permeability in the RA site, which allows nanocarriers to passively accumulate through the ELVIS effect (extravasation through leaky vasculature and subsequent inflammatory cell-mediated sequestration), which is similar to the EPR effect observed in solid tumors [6]. Based on the mechanisms, nanocarriers have been demonstrated to efficiently deliver anti-inflammation drugs to joints and manage the progression of disease. Chen et al. [7] developed an RGD peptide-modified MTX-loaded Pd nanosheet (Pd-Cys@MTX@RGD) to treat RA. Near-infrared laser irradiation increased the temperature of the inflamed paws, and MTX was rapidly released from the nanosheets, thus enhancing its therapeutic efficacy *in vivo*. Yang et al. [8] prepared a neutrophil membrane-coated F127 polymer nanoparticle. The nanoparticle can target synovitis, effectively inhibit synovial inflammation and reduce joint injury through macrophage polarization reprogramming. Feng et al. [9] designed dexamethasone-loaded zeolitic imidazolate framework nanoparticles modified by dextran sulfate that can selectively deliver dexamethasone to inflammatory tissue via scavenger receptors.

Many types of cells, including B cells, T cells, fibroblast-like synoviocytes (FLSs), macrophages and chondrocytes, infiltrate the synovial membranes of RA patients. These cells interact with each other, secrete various inflammatory factors, and contribute to the destruction of articular cartilage [6,10,11]. Furthermore, blood vessel proliferation and inflammatory cell infiltration lead to increased oxygen consumption by the cells. Notably, hypoxia is one of the most typical features of the internal environment of RA. Hypoxia induces the production of reactive oxygen species (ROS), and these free radicals can accelerate the progression of inflammation, damaging the joints [4,12]. Macrophages are mainly polarized to the M1 subtype and can secrete proinflammatory factors to maintain and aggravate synovial inflammation and cartilage destruction. Hypoxia-inducible factor (HIF-1 $\alpha$ ) is overexpressed in hypoxic-inflammatory microenvironments, enhancing the transcription and activation of hundreds of genes regulating inflammation, fibroblast fibrosis and angiogenic responses, activating fibroblasts and promoting disease progression [13,14]. Therefore, eliminating the overproliferation of inflammatory cells, improving the hypoxic microenvironment and inducing the M1 to M2 macrophage phenotype transition are considered important strategies to alleviate RA symptoms.

Photothermal therapy (PTT) is a minimally invasive therapy that uses light and photosensitizers to exert photothermal effects. The photothermal conversion agents effectively convert near-infrared (NIR) light penetrating the inflamed joint into localized heat, thereby destroying the diseased region [15–17]. NIR laser irradiation can raise the local temperature to above 42 °C and effectively ablate inflammatory cells and promote their apoptosis [18,19]. Polydopamine (PDA) is a new multifunctional biomimetic

polymer inspired by adhesion proteins in mussels. Because of its good biocompatibility and strong NIR absorption ability, it has been widely considered [20,21]. In addition, PDA has many phenolic hydroxyl and amino groups on its surface that can scavenge ROS and protect joint cartilage from damage [22,23].

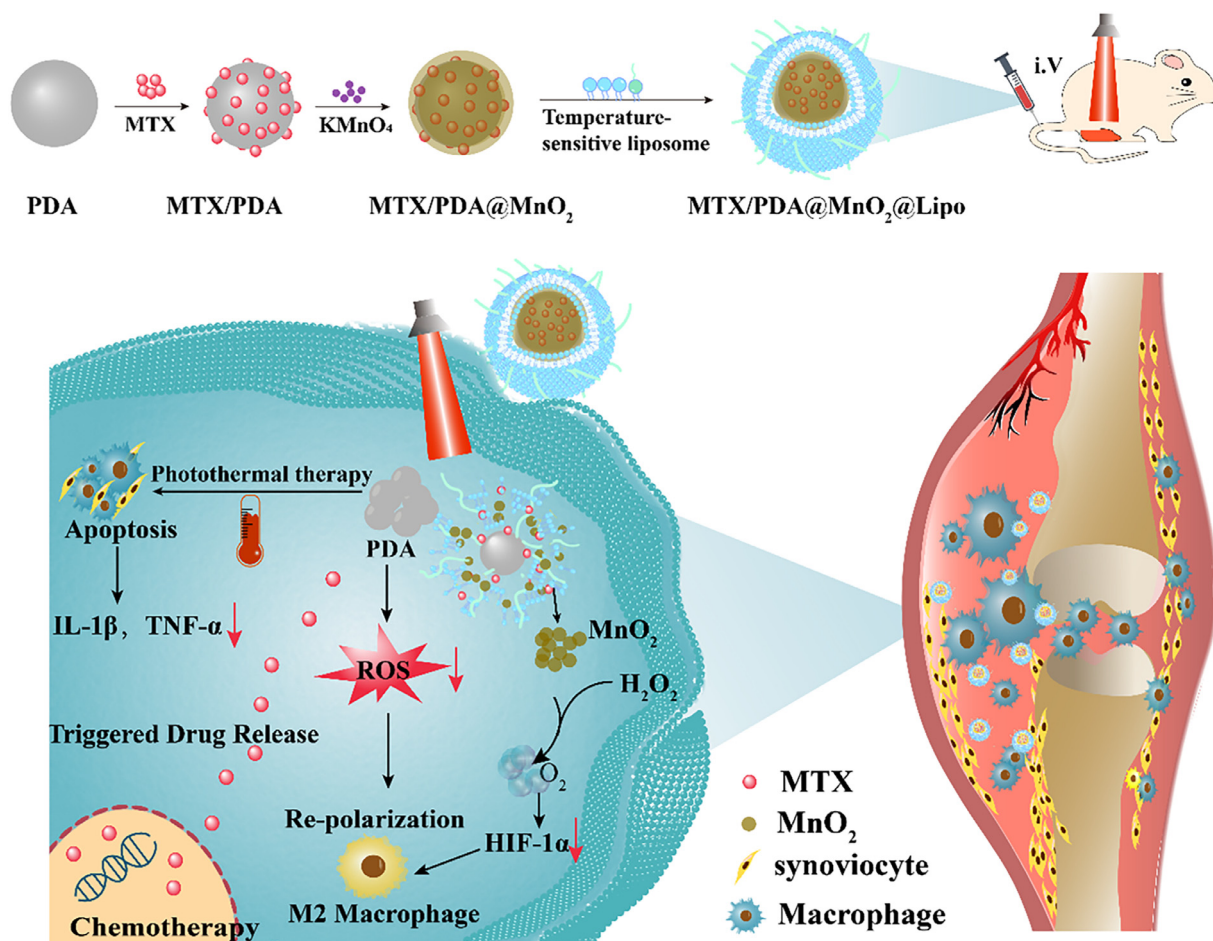
The strategy of RA treatment based on oxygen production by catalase-like enzymes has shown strong potential for application. Catalase-like nanomaterials react with H<sub>2</sub>O<sub>2</sub> to generate oxygen through a self-sufficient process. Metal-based catalase-like nanomaterials include calcium dioxide (CaO<sub>2</sub>), manganese dioxide (MnO<sub>2</sub>), platinum nanoenzymes (Pt NPs) and cerium dioxide (CeO<sub>2</sub>) [24]. Among these nanomaterials, MnO<sub>2</sub> exhibits favorable biocompatibility and can catalyze excess H<sub>2</sub>O<sub>2</sub> to produce oxygen, providing a good effect in the improvement of hypoxic diseases. MnO<sub>2</sub> has extensive antioxidant activities and can inhibit the formation of free radicals and clear ROS *in vivo*. Furthermore, nanocarriers containing MnO<sub>2</sub> are prone to degradation in H<sub>2</sub>O<sub>2</sub>-rich environments, which help to achieve responsive drug release [25].

In the present study, H<sub>2</sub>O<sub>2</sub>-responsive MTX/PDA@MnO<sub>2</sub>@Lipo (MPM@Lipo) was prepared and characterized. As shown in Scheme 1, the prepared MPM@Lipo selectively accumulated in adjuvant-induced arthritis (AIA) joints through the inflammation-targeting ELVIS mechanism and was phagocytosed by inflammatory cells. The PDA was able to scavenge ROS and directly ablate inflammatory cells due to its excellent NIR absorption ability. MnO<sub>2</sub> can induce the decomposition of H<sub>2</sub>O<sub>2</sub> to H<sub>2</sub>O and oxygen, alleviate hypoxia in inflamed joints, and achieve H<sub>2</sub>O<sub>2</sub>-responsive MTX release. After heating, MPM@Lipo can destabilize the structure of thermosensitive liposomes and synergistically enhance MTX and oxygen release at the site of inflammation to minimize RA symptoms. In summary, MPM@Lipo has significant potential as an inflammatory microenvironment modulator in the treatment of RA.

## 2. Materials and methods

### 2.1. Materials

Lipopolysaccharide (LPS) and MTX were obtained from Sigma Technology Co., Ltd. Dopamine hydrochloride was purchased from Energy-chemical Technology Co., Ltd (Anhui, China). 1,2-dipalmitoyl-sn-glycerol-3-phosphocholine (DPPC), 1,2-distearoyl-sn-glycerol-3-phosphocholine (DSPC) and N-(Carbonyl-methoxypolyethyleneglycol-2000)-1,2-distearoyl-sn-glycerol-3-phosphoethanolamine sodium salt (DSPE-mPEG<sub>2000</sub>) were obtained from Avital Pharmaceutical Technology Co., Ltd (Shanghai, China). Rhodamine B (RhB) and DCFH-DA were purchased from Solarbio Co., Ltd (Beijing, China). Total mRNA extraction kits, qRT-PCR and TOPreal SYBR Green premix were purchased from Yeasen Biotech Co., Ltd (Shanghai, China). The primary antibodies for phosphatidylinositol-3 kinase (PI3K), p-PI3K, HIF-1 $\alpha$ , CD206, iNOS, protein kinase (AKT), p-AKT, and  $\beta$ -actin secondary antibodies were provided by Abcam co. Ltd. Complete Freund's adjuvant was obtained from Chondrex (WA, USA).



**Scheme 1 – Schematic illustration of the construction of MPM@Lipo and their application for RA therapy and related mechanisms of MPM@Lipo against RA.**

## 2.2. Preparation of MPM@Lipo

Dopamine hydrochloride can spontaneously form PDA nanoparticles under alkaline conditions in an oxygenated environment [26,27]. Dopamine hydrochloride (80 mg) was dissolved in 60 ml deionized water (pH 9.0) for 5-h reaction at 50 °C and 500 r/min. During the reaction, the solution gradually changed from transparent and colorless to brownish-black. PDA nanoparticles were collected by centrifugation at room temperature and washed with deionized water. Then, the MTX solution (5 mg/ml, 1 ml) was dispersed in the PDA nanoparticles (2 mg/ml, 10 ml) and stirred for 24 h to obtain MTX/PDA. Finally, the MTX/PDA nanoparticles were mixed with  $\text{KMnO}_4$  solution (10 mg/ml, 1 ml) under sonication for 5 min and stirred for 4 h at 40 °C. The uncoated MTX and  $\text{MnO}_2$  were purified by dialysis to obtain MTX/PDA@ $\text{MnO}_2$  (MPM) nanoparticles.

Temperature-sensitive liposome was prepared by the reverse-phase evaporation method [28,29]. DPPC, DSPC, cholesterol and DSPE-PEG<sub>2000</sub> with a molar ratio of 50:12:32:6 were used in the liposomal formulation. These lipids were dissolved in chloroform (3 ml), and 2 ml MPM nanoparticles (5 mg/ml) was added. The mixture was evaporated to the gel state at 40 °C under reduced pressure. After PBS was added, a

lipid mixture (10 mg/ml) was formed and sonicated in an ice bath, and extruded (Avanti Polar Lipids Inc., USA) to obtain MPM-loaded liposomes (MPM@Lipo).

## 2.3. Characterization of MPM@Lipo

The Zetasizer Nano (ZS 3000, USA) and transmission electron microscopy (TEM, FEI) were used to detect the particle size, zeta potential and morphology of PDA, MTX/PDA, MPM and MPM@Lipo. The characteristic absorption peaks of MTX, PDA, MTX/PDA and MPM were measured by a UV-vis spectrophotometer (UV-1800, Agilent) and FTIR spectrophotometer (Nicolet 6700, Thermo Fisher Scientific Inc.). The chemical composition of MPM was analyzed by an X-ray photoelectron spectrometer (XPS, FEI). The Mn concentration was detected by inductively coupled plasma-optical emission spectrometry (ICP-OES, Perkin Elmer). The stability of MPM@Lipo was investigated at 4 °C for 60 d HPLC (Shimadzu, Kyoto, Japan) was used to determine the content of MTX in the nanoparticles at a wavelength of 302 nm. The encapsulation efficiency and loading efficiency were determined using the following equations:

Encapsulation efficiency (%)

$$= \text{MTX encapsulated in the liposomes} / \text{MTX fed} \times 100\%$$

Loading efficiency (%)

$$= \frac{\text{MTX encapsulated in the liposomes}}{\text{total liposomes}} \times 100\%$$

#### 2.4. Hemolysis test

Two percent (v/v) red blood cell suspensions were prepared with reference to published literature [30]. Controls were 0.9% NaCl (negative) and 0.1% Triton X-100 (positive). The erythrocyte solutions were incubated with different concentrations (5–200 µg/ml) of MPM@Lipo at 37 °C for 4 h. The supernatants of each group after centrifugation were analyzed at OD 541 nm to calculate the hemolysis percentage.

#### 2.5. In vitro MTX release

The MTX release from MPM@Lipo was studied using the dialysis method with the following experimental groups: In the MPM@Lipo group, 2 ml MPM@Lipo (MTX: 0.5 mg) was placed into a dialysis bag and immersed in 40 ml pH 7.4 PBS; In the MPM@Lipo+Laser group, MPM@Lipo were irradiated by an 808 nm NIR laser (1.5 W/cm<sup>2</sup>) for 10 min and then immersed in pH 7.4 PBS; In the MPM@Lipo+Laser+H<sub>2</sub>O<sub>2</sub> group, MPM@Lipo irradiated with a laser and were placed in pH 7.4 PBS with 10 mmol/l H<sub>2</sub>O<sub>2</sub>. Each release system was continuously shaken on a rotating shaker at 100 r/min. Release samples were withdrawn at 0.5 h, 1 h, 2 h, 3 h, 6 h, 9 h, 12 h and 24 h, and were detected using HPLC at 302 nm.

#### 2.6. In vitro photothermal performance

The temperature changes of PBS, MTX/PDA, MPM and MPM@Lipo were recorded after NIR laser irradiation (1.5 W/cm<sup>2</sup>), and the photothermal properties were evaluated. To investigate the influence of the MPM@Lipo concentration on the photothermal conversion efficiency, the temperature changes upon NIR laser (1.5 W/cm<sup>2</sup>) irradiation for 720 s were monitored by an infrared thermal camera (RX-300; Bufan, China). An on/off-cycle irradiation experiment was performed to evaluate the photothermal stability of MPM@Lipo (50 µg/ml). MPM@Lipo was irradiated (1.5 W/cm<sup>2</sup>) to reach a stable temperature, and the laser was removed to allow the sample to cool to room temperature. This procedure was repeated for multiple cycles. Additionally, the temperature change in MPM@Lipo (50 µg/ml) was imaged by an infrared thermal camera.

#### 2.7. H<sub>2</sub>O<sub>2</sub> decomposition and in vitro oxygen generation

The titanium sulfate microplate method was used to evaluate the amount of H<sub>2</sub>O<sub>2</sub> consumed by MTX/PDA, MPM and MPM@Lipo. MTX/PDA, MPM, and MPM@Lipo (100 µg/ml) were mixed with a certain amount of H<sub>2</sub>O<sub>2</sub>. Then, Ti(SO<sub>4</sub>)<sub>2</sub> solution was dropped in the above mixture and incubated for 0.5 h. The supernatants were measured at 405 nm (BioTek Epoch).

The amount of oxygen generated from the nanoparticles was detected by a dissolved oxygen meter (Rex Electric Chemical), which was monitored every 60 s by adding 100 µg/ml MTX/PDA, MPM or MPM@Lipo to PBS containing 100 µmol/l H<sub>2</sub>O<sub>2</sub> with continuous stirring.

#### 2.8. Cytotoxicity study

RAW264.7 cells were obtained from Zhejiang Meisen Cell Technology Co., Ltd. LPS-activated RAW264.7 were obtained by stimulating RAW264.7 cells with 100 ng/ml LPS for 12 h. RA-FLSs, are the human rheumatoid arthritis fibroblast-like synovial cells, were obtained from Guangzhou Genio Biotechnology Co., Ltd. DMEM containing 10% FBS was used to culture the cells at 37 °C in a 5% CO<sub>2</sub> environment. Cytotoxicity was studied by MTT assay. Various concentrations of PDA, PDA@MnO<sub>2</sub> or PDA@MnO<sub>2</sub>@Lipo were cocultured with RA-FLSs and RAW264.7 cells for 24 h. Subsequently, MTT solution was added and treated for 4 h. 150 µl DMSO was used to dissolve the purple precipitate. The samples were measured at 570 nm.

RA-FLSs, RAW264.7 and LPS-activated RAW264.7 cells were used to study the cytotoxicity of MTX and MTX-containing formulations. Cells were seeded in 96-well plates and incubated with MTX, MTX/PDA, MPM, MPM@Lipo or MPM@Lipo +Laser for 24 h. MPM@Lipo +Laser treated cells were irradiated with a 1.5 W/cm<sup>2</sup> NIR laser for 10 min after 6-h incubation. The following steps were the same as above.

LPS-activated RAW264.7 and RA-FLSs were inoculated in 12-well plates, and 10 µg/ml MTX, MTX/PDA, MPM, MPM@Lipo or MPM@Lipo+Laser was added and incubated for 24 h. The cells were then stained with Calcein AM/PI for 30 min in the dark and imaged by a fluorescence microscope (Leica, Germany). Untreated cells were selected as a blank group.

#### 2.9. Cellular uptake study

RhB-loaded nanoparticles, including RhB/PDA, RhB/PM and RhB/PM@Lipo, were prepared. RhB, RhB/PDA, RhB/PM or RhB/PM@Lipo were cocultured with RA-FLSs and LPS-activated RAW264.7 cells for 2 h, respectively. Then, the cells were labeled with Hoechst 33,342 and observed by fluorescence microscope. Uptake of the RhB-loaded nanoparticles was also determined by flow cytometry (Backman, CytoFLEX LX).

#### 2.10. ROS scavenging activity

LPS-activated RAW264.7 cells or RA-FLSs were seeded in 12-well plates and incubated with MTX, MTX/PDA, MPM, MPM@Lipo or MPM@Lipo+Laser for 24 h. Thereafter, the cells were further treated with DCFH-DA (10 µmol/l) for 30 min at 37 °C, and imaged by fluorescence microscope. The collected cells were also examined for intracellular ROS fluorescence intensity by flow cytometry.

#### 2.11. Western blotting and real-time RT-PCR

LPS-activated RAW264.7 cells were treated with 10 µg/ml MTX, MTX/PDA, MPM, MPM@Lipo or MPM@Lipo+Laser for 24 h in a hypoxic chamber. The total proteins were extracted, and the protein expression of PI3K, p-PI3K, HIF-1 $\alpha$ , AKT and p-AKT were investigated by Western blotting. LPS-activated RAW264.7 cells were treated using the same method used for Western blotting. The expression of HIF-1 $\alpha$ , TNF- $\alpha$ , IL-6, IL-1 $\beta$ , iNOS, CD206 and Arg-1 gene were determined by RT-PCR.

The relative levels of mRNA expression were analyzed by the  $2^{-\Delta\Delta CT}$  method and normalized to GAPDH expression.

### 2.12. Immunofluorescence staining

The cells were treated using the same method used for Western blotting. The cells were immobilized with 4% paraformaldehyde, incubated with primary antibodies (HIF-1 $\alpha$ , iNOS or CD206) overnight, incubated with fluorescent secondary antibody for 1 h, and observed under a fluorescence microscope.

### 2.13. Pharmacokinetics study

Male Sprague-Dawley (SD) rats were administered with free MTX or MPM@Lipo (MTX dose = 2.5 mg/kg) via intravenous injection. Blood samples were collected in heparinized tubes (anticoagulant) at preset intervals of 0.05, 0.167, 0.5, 1, 3, 6, 12 and 24 h. The MTX concentration in plasma was determined by liquid chromatography–mass spectrometry (LC–MS/MS, Agilent) as previously reported [31].

### 2.14. Fluorescence imaging and photothermal effect in vivo

#### 2.14.1. Establishment of the AIA rat model

All animal experiments in this study were conducted following approved protocols by the institutional animal care and use committee of Fujian Medical University (SCXK (Min) 2016–0002). The AIA arthritis model was induced in SD rats according to a literature method [30]. 100  $\mu$ l complete Freund's adjuvant was injected into the right posterior paws of the rats by intraplantar injection. The rat's ankle was checked every day, and it showed significant swelling two weeks after the injection.

#### 2.14.2. In vivo targeting evaluation

DIR-loaded PDA@MnO<sub>2</sub>@Lipo (DIR/PM@Lipo) was prepared using the same method used for MPM@Lipo. AIA rats were injected with free DIR or DIR/PM@Lipo (50  $\mu$ g/kg) through the tail vein. The hind limbs of rats were photographed at 1, 3, 9 and 24 h using the IVIS system (Caliper, USA). The joint and main organs were dissected for *in vitro* fluorescence imaging at 24 h.

#### 2.14.3. Photothermal effect of MPM@Lipo in vivo

For *in vivo* photothermal experiments, AIA rats were injected intravenously with MPM@Lipo (concentrations of MTX 1 mg/kg). After 24 h of administration, the ankle joints were irradiated by NIR laser (10 min). During the process of laser irradiation, an infrared thermal imaging system was used to record photothermal images of joints at different time points. The MPM@Lipo was not exposed to NIR as the control group.

### 2.15. In vivo anti-arthritis effect

#### 2.15.1. Anti-inflammatory efficacy evaluation

The AIA rats were injected intravenously with saline, MTX, MPM, or MPM@Lipo (MTX: 1 mg/kg). The ankle joints of the MPM@Lipo+Laser group were administered NIR laser (1.5 W/cm<sup>2</sup>, 10 min) irradiation after 12 h of tail vein injection

of MPM@Lipo. Normal rats were used as the control group. Treatments were given on Day 15, 18, 21, 24, 27, 30 and 33 after immunization. The paw thickness, paw volume and arthritis index were measured every 3 d during the treatment period. Rat hind paw thicknesses were carefully measured with Vernier calipers. Rat hind paw volumes were measured by a volume meter (YLS-7C, Jinan). Arthritis was scored according to the degree of swelling of the joints. Based on previous reports [32], the paw scores were categorized from 0 (normal paw) to 4 (severe edema with joint stiffness and redness).

#### 2.15.2. Quantification of cytokines and histopathology of the ankle joints

The rats were euthanized on Day 33 after arthritis induction. Joint tissue was stripped and the concentration of inflammatory factors was analyzed by ELISA. The other inflamed joints were fixed in 4% formaldehyde and then decalcified in 10% EDTA solution. Subsequently, the fixed ankle joints were embedded in paraffin, sectioned and stained. Ankle sections were stained with H&E and Safranin O to observe inflammatory cell infiltration and the loss of cartilage proteoglycans. The expression of HIF-1 $\alpha$  was observed by immunofluorescence staining.

#### 2.15.3. Safety evaluation

The body weights of all rats were recorded during the experiment. On Day 33, rat liver and kidney function tests were performed on a fully automated biochemical analyzer (Beckman Coulter). The main organs were removed, embedded in paraffin and sectioned for histopathological observations by H&E staining. Histological lesions were evaluated and photographed using a microscope.

### 2.16. Statistical analysis

All data are shown as mean  $\pm$  standard deviation (SD) of at least three separate experiments unless otherwise indicated. Student's t-test and one-way analysis of variance (ANOVA) were applied to determine differences between groups. A value of  $P < 0.05$  was considered statistically significant.

---

## 3. Results and discussion

### 3.1. Preparation and characterization of MPM@Lipo

Eliminating hyperproliferating inflammatory cells and improving the hypoxic microenvironment are considered important therapeutic strategies for relieving RA symptoms. Thus, this study presents an H<sub>2</sub>O<sub>2</sub>-responsive MPM@Lipo combined PTT for RA therapy. The PDA nanoparticles were prepared by the self-polymerization of dopamine hydrochloride under alkaline conditions, and MTX was loaded onto the PDA nanoparticles (MTX/PDA nanoparticles) by physical adsorption. Subsequently, a MnO<sub>2</sub> layer was formed on the PDA nanoparticle (MTX/PDA@MnO<sub>2</sub>, MPM) surface due to the redox reaction between PDA and KMnO<sub>4</sub> under neutral conditions. Finally, the MPM nanoparticles were coated with temperature-sensitive liposomes (MPM@Lipo) to prevent drug leakage and improve the stability of the

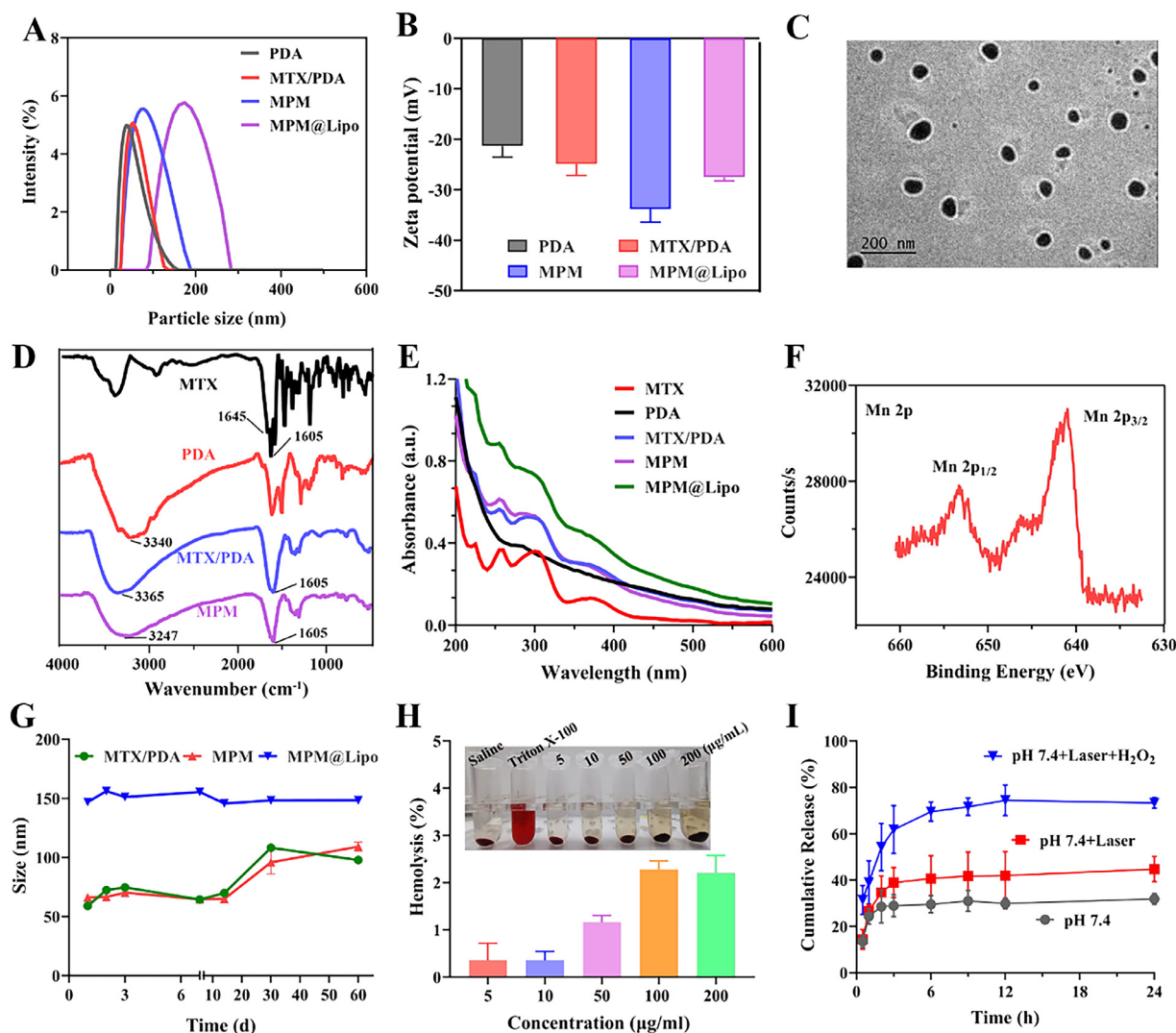


**Fig. 1** – In vitro characterization of MPM@Lipo. (A) Particle size and size distribution of PDA, MTX/PDA, MPM and MPM@Lipo; (B) Zeta potential diagram of PDA, MTX/PDA, MPM and MPM@Lipo; (C) Representative TEM images of MPM@Lipo, scale bar=200 nm; (D) FTIR spectra, (E) UV-vis absorbance spectra, (F) XPS spectrum of MPM; (G) Storage stability of MTX-loaded nanoparticles in deionized water at 4 °C within 60 d ( $n = 3$ ); (H) The hemolysis percentage of MPM@Lipo; (I) In vitro release of MTX from MPM @Lipo under different conditions ( $n = 3$ ).

nanoparticles. In this study, the effects of the mass ratios of MTX to PDA, MTX/PDA and  $\text{KMnO}_4$ , reaction temperature, reaction time, and MPM to lipid mass ratio on particle size and encapsulation efficiency were investigated using single-factor experiments. The results showed that MPM@Lipo had a suitable particle size and higher encapsulation efficiency when the mass ratio of MTX to PDA is 1/10, the mass ratio of MTX/PDA to  $\text{KMnO}_4$  is 1/3, the temperature and time are 25 °C and 4 h, and the MPM/lipid ratio is 2/3. The particle sizes of PDA, MTX/PDA, MPM, and MPM@Lipo were  $56.50 \pm 1.04$  nm,  $56.73 \pm 0.15$  nm,  $71.50 \pm 0.26$  nm and  $163.14 \pm 16.22$  nm, respectively (Fig. 1A). The corresponding zeta potentials were  $-21.28 \pm 2.24$  mV,  $-24.90 \pm 2.26$  mV,  $-33.86 \pm 2.54$  mV and  $-27.44 \pm 0.78$  mV, respectively (Fig. 1B). The TEM images showed that PDA and MPM had good dispersion and a uniform particle size (Fig. S1). MPM@Lipo is an excellent drug carrier with a particle size of less than 200 nm that can be

used for targeted drug delivery through vascular leakage and retention but is not cleared in the spleen or kidney. As shown in Fig. 1C, MPM@Lipo were spherical, uniform in size, and well dispersed without precipitation or aggregation. Moreover, the nanoparticles had a thin layer on the surface, which was presumed to be the hydration layer of the PEG-modified liposomes. The drug loading efficiency in MPM@Lipo was  $5.63\% \pm 0.33\%$ , and the encapsulation efficiency was  $77.27\% \pm 0.78\%$ .

In the FTIR spectra of MTX, the typical absorption at  $1645 \text{ cm}^{-1}$  and  $1605 \text{ cm}^{-1}$  belonged to the overlapping of C = O stretching and N-H band stretching vibrations. The characteristic wide peak at  $3400\sim 3200 \text{ cm}^{-1}$  could be ascribed to the -OH of PDA. In the FTIR spectra of MTX/PDA and MPM, the characteristic peaks of PDA ( $3340 \text{ cm}^{-1}$ ) and MTX ( $1605 \text{ cm}^{-1}$ ) appeared, which demonstrated the successful adsorption of MTX on MTX/PDA or MPM (Fig. 1D). As shown

in Fig. 1E, MTX/PDA and MPM exhibited obvious UV-visible absorption peaks at 302 nm, which are characteristic of MTX, further confirming that MTX was successfully loaded onto the PDA nanoparticles. The peak intensity of the MPM@Lipo at 302 nm was reduced, probably due to the masking of MTX by the outer liposomes. The signal peak of Mn was clearly observed by XPS (Fig. S2). The high-resolution XPS spectrum (Fig. 1F) showed that the characteristic peak at 654.2 eV corresponds to Mn(IV) 2p<sub>2/3</sub> spin-orbit peaks and that the peak at 642.4 eV corresponds to Mn(IV) 2p<sub>1/2</sub> spin-orbit peaks of MnO<sub>2</sub>. This result confirmed the deposition of MnO<sub>2</sub> on the surface of the PDA nanoparticles. The doping level of Mn ions in MPM was measured to be approximately 127.87 mg/g (w/w) by ICP-OES.

The *in vitro* stability of the nanoparticles was investigated using particle size as an index. The MTX/PDA and MPM nanoparticles increased in size after 2 weeks of storage at 4 °C, while MPM@Lipo showed almost no change in size after 60 days of storage (Fig. 1G). The excellent stability of MPM@Lipo may be due to the hydrophilic shell of the PEGylated liposome, which enhanced the dispersion of MPM@Lipo in aqueous solution. As described in Fig. 1H, erythrocytes showed significant hemolysis in 0.1% Triton X-100 solution. After incubation of 5–200 µg/ml MPM@Lipo with erythrocyte suspensions for 4 h, the hemolysis rate was less than 3%, indicating that MPM@Lipo was only very slightly hemolytic in this concentration range. These data indicated that MPM@Lipo has good hemocompatibility *in vitro* and can be used for intravenous injection.

### 3.2. *In vitro* MTX release

As depicted in Fig. 1I, the cumulative release of MTX from MPM@Lipo in pH 7.4 PBS was less than 30% within 24 h. After laser irradiation, the cumulative drug release increased to 45%. This may be due to the photothermal effect produced by PDA, which increased the temperature and particle size of MPM@Lipo (Fig. S3). However, the structural integrity of MPM@Lipo was well maintained, resulting in a rapid release of only some MTX. In the simulated joint inflammation microenvironment (pH 7.4 PBS+H<sub>2</sub>O<sub>2</sub>+Laser), the cumulative drug release increased to 73%. The massive release of oxygen destroyed the integrity of the MPM@Lipo, allowing MTX to be rapidly released in a short time. Such responsive drug release behavior helps to reduce the release of MTX from MPM@Lipo under normal physiological conditions and increase the accumulation of drugs at the inflammation site, thereby reducing the occurrence of side effects. These results confirmed that the prepared MPM@Lipo had the characteristics of controlled drug release in the inflammatory microenvironment and a near-infrared laser response, which was conducive to the rapid triggering of drug release in inflamed joints [33].

### 3.3. Photothermal properties assay

To examine the photothermal performance of MPM@Lipo, a series of photothermal experiments were conducted under 808 nm laser irradiation. Fig. 2A shows the curves

of the temperature changes of the PBS, MTX/PDA, MPM and MPM@Lipo solutions after laser (1.5 W/cm<sup>2</sup>, 12 min) irradiation. The temperature of PBS remained almost unchanged, while the temperatures of the MTX/PDA, MPM, and MPM@Lipo solutions rapidly increased with prolonged irradiation time, reaching approximately 46.6 °C within 12 min. The results showed that the adsorption of MTX and the outer liposomal layer had almost no effect on the temperature change of PDA. The photothermal performance of MPM@Lipo exhibited a significant concentration dependence (Fig. 2B). Within a certain time, the temperature of the MPM@Lipo solution increased with increasing concentration from 25 to 50 µg/ml. After comprehensive consideration, 50 µg/ml MPM@Lipo was finally selected for subsequent experiments. Furthermore, the curve of the rise in the temperature of the MPM@Lipo aqueous solution under three irradiation-cooling cycles is shown in Fig. 2C. The photothermal performance of MPM@Lipo presented no evident regression after three cycles of heating by laser exposure (808 nm, 1.5 W/cm<sup>2</sup>) and cooling, indicating the excellent photothermal stability and repeated usability of MPM@Lipo. The photothermal conversion efficiency of MPM@Lipo was approximately 36.43% (Fig. 2D) based on a previously reported method [34]. The infrared (IR) camera recorded a significant temperature increase in 12 min (Fig. 2E), which visually indicated the better photothermal properties of MPM@Lipo. The results of photothermal experiments showed that the temperature of the MPM@Lipo solution could increase rapidly, providing the possibility of inhibiting synovial proliferation through thermotherapy.

### 3.4. Decomposition of H<sub>2</sub>O<sub>2</sub> and production of oxygen

Compared with normal joints, ROS levels were significantly increased in the inflammatory microenvironment of RA. ROS scavenging is an important strategy for RA treatment. Several research reports have shown that PDA nanoparticles can not only act as reducing agents for redox reactions with ROS but also act as catalysts to trigger the decomposition of H<sub>2</sub>O<sub>2</sub> [22]. In addition, MnO<sub>2</sub> has a peroxidase-like activity that decomposes H<sub>2</sub>O<sub>2</sub> to produce water and oxygen. In pH 7.4 buffer, the same concentration of MTX/PDA, MPM and MPM@Lipo (100 µg/ml) decomposed 28.3%, 58.9% and 56.95% H<sub>2</sub>O<sub>2</sub> in 0.5 h, respectively (Fig. 2F). With increasing MPM@Lipo concentration, the decomposition of H<sub>2</sub>O<sub>2</sub> increased (Fig. S4). The PDA and MnO<sub>2</sub> in the nanoparticles had a synergistic ability to decompose H<sub>2</sub>O<sub>2</sub>. The decomposition efficiency was not affected by liposome encapsulation, and MPM@Lipo had an excellent ability to decompose H<sub>2</sub>O<sub>2</sub>.

The peroxidase activities of MPM and MPM@Lipo were evaluated by measuring the amount of dissolved oxygen and observing oxygen bubbles. MPM and MPM@Lipo rapidly generated a large amount of oxygen in a short period, and the dissolved oxygen values reached 18.9 mg/l and 19.7 mg/l after 400 s, respectively (Fig. 2G). However, no obvious bubbles were observed in the MTX/PDA solution at the same concentration. These results indicated that MPM and MPM@Lipo with peroxidase-like activity could effectively decompose endogenous H<sub>2</sub>O<sub>2</sub> to generate oxygen.

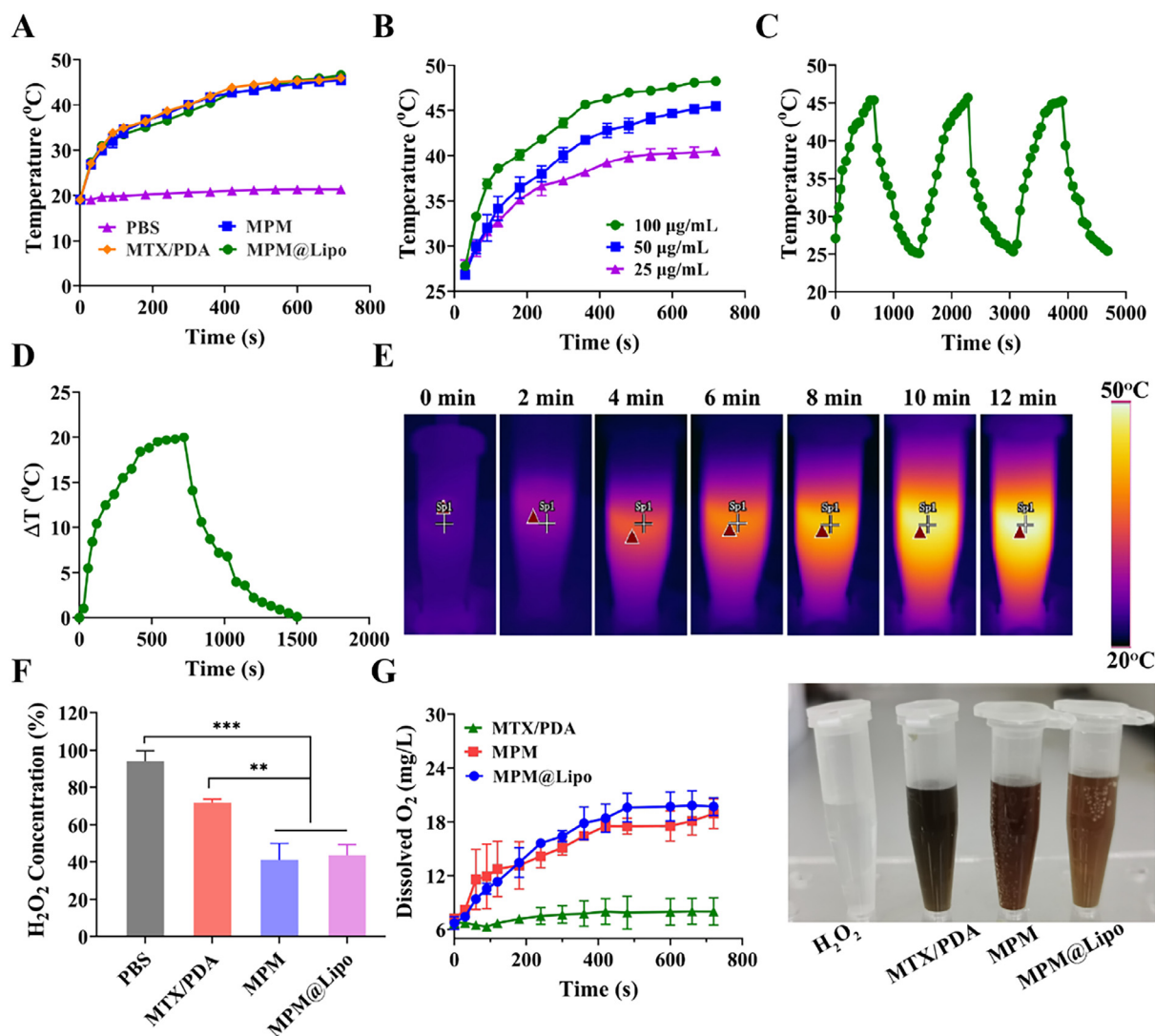


**Fig. 2** – Evaluation of photothermal performance and oxygen production of MPM@Lipo. (A) The temperature changes of PBS, MTX/PDA, MPM and MPM@Lipo after laser irradiation ( $1.5 \text{ W/cm}^2$ ) for 720 s. (B) The temperature changes in the MPM@Lipo at various concentrations (from 25 to  $100 \text{ }\mu\text{g/ml}$ ) after laser irradiation ( $1.5 \text{ W/cm}^2$ ) for 720 s. (C) The photothermal stability of the MPM@Lipo under three irradiation-cooling cycles. (D) The photothermal curve of MPM@Lipo ( $50 \text{ }\mu\text{g/ml}$ ) by turning the NIR laser on and off. (E) Real time thermal images of MPM@Lipo ( $50 \text{ }\mu\text{g/ml}$ ) during NIR irradiation ( $1.5 \text{ W/cm}^2$ ). (F) Decomposition of  $\text{H}_2\text{O}_2$  in the presence of MTX/PDA, MPM and MPM@Lipo. (G) Generation curves of  $\text{O}_2$  and corresponding photographs of  $\text{O}_2$  bubbles generated in  $100 \text{ }\mu\text{mol/l}$   $\text{H}_2\text{O}_2$  solution in the presence of MTX-loaded nanoparticles ( $n = 3$ ).

### 3.5. MTT assays

Inflammatory cells were selected to detect the therapeutic effects of MTX and MTX-loaded nanoparticles at the cellular level. RA-FLSs are the main effector cells that cause cartilage injury. Synovial cells prolifically transform the synovial membrane from a relatively static cell-free structure to aggressive tissue rich in many immunoreactive cells with a strong proliferative capacity [35]. Macrophages are crucial in the pathophysiological response of arthritis and are highly active in inflamed sites. RAW264.7 cells have a classical proinflammatory (M1) phenotype (LPS-activated) and an anti-inflammatory (M2) phenotype. If proinflammatory factors are

predominant, the balance is disturbed, and RA develops. Thus, these two cell phenotypes are essential for maintaining homeostasis in the internal RA environment [36]. After incubation with PDA, PDA@MnO<sub>2</sub>, and PDA@MnO<sub>2</sub>@Lipo for 24 h, the cell survival rates were greater than 80%. PDA nanoparticles did not significantly affect the proliferation of RA-FLSs or RAW264.7 cells (Fig. 3A), indicating that this material was nontoxic and had good biocompatibility.

RA-FLSs were incubated with different concentrations of MTX, MTX/PDA, MPM, MPM@Lipo and MPM@Lipo+Laser for 24 h, along with a decrease in all MTX formulation concentrations, and cell proliferation was obviously improved (Fig. 3B). The corresponding IC<sub>50</sub> values were  $155.8 \pm 2.19$ ,

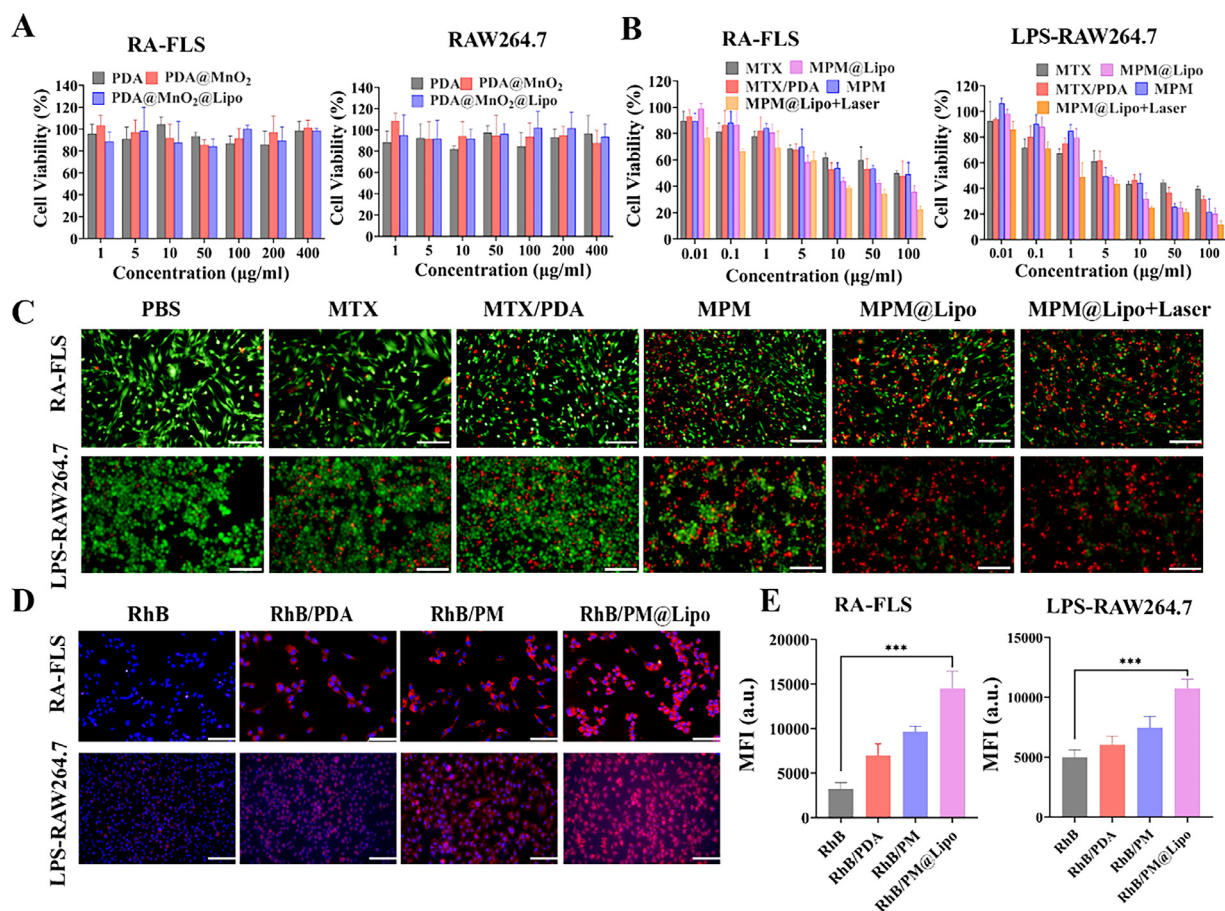


**Fig. 3** – Proliferation inhibiting effects and intracellular uptake. (A) The cell viability of RA-FLSs cells and RAW 264.7 cells after 24 h incubation with PDA, PDA@MnO<sub>2</sub> and PDA@MnO<sub>2</sub>@Lipo (*n* = 3). (B) The cell viability of RA-FLSs cells and LPS- activated RAW 264.7 cells treated with different concentrations of MTX, MTX/PDA, MPM, MPM@Lipo and MPM@Lipo+Laser for 24 h (*n* = 3). (C) Fluorescence microscope images of calcein AM/PI staining of RA-FLSs cells and LPS- activated RAW 264.7 cells treated with different group. Green and red represent live and dead cells, respectively, scale bar= 100 µm. (D) Fluorescent microscopy images of RhB, RhB/PDA, RhB/PM and RhB/PM@Lipo in RA-FLSs cells and LPS-activated RAW 264.7 cells (2 h). The nuclei were stained with Hoechst 33,342 (blue), scale bar = 100 µm. (E) Fluorescence intensity was quantified by flow cytometry (*n* = 3). \*\*\**P* < 0.001.

59.28 ± 1.78, 59.39 ± 1.78, 16.44 ± 1.22 and 3.77 ± 0.58 µg/ml, respectively. Furthermore, after treatment with MTX, MTX/PDA, MPM, MPM@Lipo and MPM@Lipo+Laser, LPS-activated RAW264.7 cells showed cell viability results similar to those obtained with RA-FLSs. The IC<sub>50</sub> values were 13.97 ± 1.15, 11.67 ± 1.07, 7.81 ± 0.89, 5.5 ± 0.74 and 1.15 ± 0.06 µg/ml, respectively. The toxicity of MPM@Lipo and MPM@Lipo+Laser to both cell lines was higher than that of the other treatments, and the highest cytotoxicity was observed in the MPM@Lipo+Laser group. The MPM@Lipo+Laser group showed high cytotoxicity, partly because PDA could ablate inflammatory cells and induce apoptosis under NIR irradiation. The cytotoxicity of PDA+Laser to LPS-activated RAW264.7 cells and RA-FLSs was significantly enhanced (Fig. S5), which proved the excellent photothermal effect of PDA under NIR irradiation.

Live-dead cell staining can visually demonstrate the ability of MTX-loaded nanoparticles to inhibit the proliferation of RA-FLSs and LPS-activated RAW264.7 cells (Fig. 3C). Cells in the

untreated group showed green fluorescence and almost no dead cells. At the same concentration, mild red fluorescence was observed in the MTX, MTX/PDA and MPM groups. Cells treated with MPM@Lipo and MPM@Lipo+Laser resulted in more cell death and more red fluorescence. Notably, MPM@Lipo showed significantly enhanced antiproliferative activity under laser irradiation, which may be attributed to the photothermal effect generated by the nanoparticles and the burst drug release under hyperthermic conditions.

A cell scratch experiment was used to investigate the inhibition of RA-FLSs migration mediated by the MTX-loaded nanoparticles, and the migratory area of the cells was quantified using Image J. As shown in Fig. S6, MTX/PDA, MPM, MPM@Lipo and MPM@Lipo+Laser exhibited excellent antimigration effects on synovial cells. Compared with the PBS group, the MTX/PDA, MPM, MPM@Lipo and MPM@Lipo+Laser groups all reduced the cell migration area by more than 40%, showing a strong inhibitory effect on cell proliferation and migration.

### 3.6. Cellular uptake

As shown in Fig. 3D, the cellular internalization of RhB, RhB/PDA, RhB/PM and RhB/PM@Lipo in RA-FLSs cells and LPS-activated RAW264.7 cells were observed by fluorescence microscopy. Only a weak fluorescence signal was observed in the free RhB group, while the RhB/PM@Lipo showed the strongest red fluorescence, followed by the RhB/PDA and RhB/PM groups. To quantify the intracellular fluorescence intensity, further verification was performed by flow cytometry. The fluorescence intensity of RhB/PDA, RhB/PM and RhB/PM@Lipo in RA-FLSs was 2.15-time, 2.98-time and 4.46-time ( $P < 0.001$ ) higher than that of free RhB, respectively (Fig. 3E and S7). The fluorescence intensity of RhB/PDA, RhB/PM and RhB/PM@Lipo in LPS-activated RAW264.7 cells increased by 1.21-fold, 1.50-fold and 2.15-fold ( $P < 0.001$ ), respectively. Uptake was significantly enhanced in the MPM@Lipo group. Moreover, the cellular uptake of RhB/PM@Lipo by RA-FLSs or LPS-activated RAW264.7 cells at 0.5, 2 and 4 h was determined. The cell uptake increased in a time-dependent manner, and RhB/PM@Lipo can be rapidly endocytosed by inflammatory cells (Fig. S8). In addition, the uptake and cytotoxicity test of MPM@Lipo on macrophages were also evaluated. The uptake in LPS-activated RAW264.7 cells was greater than that of RAW264.7 cells, and nanoparticles were more cytotoxic to LPS-activated RAW264.7 cells (Fig. S9). The results of the cytotoxicity and cell uptake assays showed that the enhanced toxicity of MTX/PDA, MPM and MPM@Lipo to inflammatory cells may be due to the increased ability of the nanoparticles to be internalized by the cells, resulting in enhanced toxicity. MPM@Lipo was more efficiently taken up by inflammatory cells, probably due to the strong similarity between the liposomes and the phospholipids on the cell membrane, which more easily fused to the cells [37].

### 3.7. ROS scavenging

The articular cavity of RA is in a state of immune activation, and the secreted inflammatory cytokines can activate oxidases and produce excessive ROS. High concentrations of ROS can quickly induce chondrocyte apoptosis and eventually cause cartilage erosion. In addition, ROS promote angiogenesis and increase oxygen consumption in the joint cavity, resulting in severe hypoxia in the joint cavity [38,39]. A great number of ROS was produced in RA-FLSs and LPS-activated RAW264.7 cells, which manifested as strong green fluorescence (Fig. 4A). As expected, after MTX/PDA, MPM, MPM@Lipo and MPM@Lipo+Laser treatment, the green fluorescence intensity was reduced to a certain extent. The ROS scavenging capacity was also further analyzed by flow cytometry (Fig. 4B and S10). The fluorescence intensity in RA-FLSs treated with MTX/PDA, MPM, MPM@Lipo and MPM@Lipo+Laser decreased by 2.53, 2.55, 2.62 and 3.89 ( $P < 0.001$ ) times than that of the PBS group, respectively. Moreover, the fluorescence intensity in LPS-activated RAW264.7 cells decreased by 1.80, 1.87, 1.85 and 2.33 ( $P < 0.001$ ) times. These results indicated that the MTX-loaded nanoparticles could

decrease the production of ROS in cells and protect the cells from ROS-induced damage. MPM@Lipo combined with NIR laser irradiation caused a synergistic enhancement in the ROS scavenging ability, which may be due to the accelerated exposure of phenolic hydroxyl and amino groups on the PDA surface under laser irradiation, which can rapidly neutralize intracellular ROS.

### 3.8. Study of hypoxia signaling pathway

The long-term chronic inflammation and hypoxic microenvironment in RA lead to increased angiogenesis, and the PI3K/AKT signaling pathway can be activated under hypoxic conditions [40]. The excessive activation of the PI3K-AKT/HIF-1 $\alpha$  signaling pathway induced by hypoxia initiates the amplification of an interrelated inflammatory signaling cascade in RA. Moreover, hypoxia is further exacerbated in the RA microenvironment due to the consumption of large amounts of oxygen in the process of ROS production, which causes an inflammatory cascade reaction that constantly amplifies inflammation in a vicious cycle [41,42]. Phosphorylated PI3K and AKT enhance the activity of HIF-1 $\alpha$ , which ultimately accelerates cell proliferation and inhibits apoptosis [43]. The Western blotting results are shown in Fig. 4C. Hypoxia and LPS resulted in increased phosphorylation levels of PI3K and AKT. The expression of p-PI3K/PI3K and p-AKT/AKT decreased after MTX and MTX-loaded nanoparticle treatment, especially after MPM@Lipo+Laser treatment ( $P < 0.05$ ). The statistical data are shown in Fig. S11.

MnO<sub>2</sub> has good peroxidase activity and is widely used to relieve intracellular hypoxia. The HIF-1 $\alpha$  expression was detected by immunofluorescence staining. After LPS stimulation and exposure to hypoxia, the green fluorescence in the cells was enhanced (Fig. 4E), indicating the HIF-1 $\alpha$  expression was upregulated. After MTX/PDA, MPM, MPM@Lipo and MPM@Lipo treatment, the green fluorescence was reduced, and the level of HIF-1 $\alpha$  was decreased. The Western blotting and RT-PCR results were consistent with the immunofluorescence staining results. HIF-1 $\alpha$  protein expression was significantly decreased after MPM@Lipo and MPM@Lipo+Laser treatment. The mRNA level of HIF-1 $\alpha$  (Fig. 4D) was increased in cells under hypoxic conditions after LPS stimulation. After incubation with MTX-loaded nanoparticles, the mRNA levels of HIF-1 $\alpha$  decreased by 25.9%, 48.2%, 48.2% and 67.6% compared with the MTX group ( $P < 0.001$ ). Among them, the MPM@Lipo+Laser group showed the best downregulation effect. The above results indicated that MPM@Lipo+Laser therapy could inhibit the excessive activation of the PI3K-AKT/HIF-1 $\alpha$  pathway, reduce the activity of HIF-1 $\alpha$ , and alleviate the inflammatory response in the joint cavity. Both MPM and MPM@Lipo had good peroxidase activity and great potential to alleviate intracellular hypoxia. MPM@Lipo + Laser downregulates the expression of phosphorylated proteins and HIF-1 $\alpha$  better than MPM and MPM@Lipo. As reported in a previous study, the temperature rise of photothermal-based nanomaterials accelerates the burst release of oxygen, which effectively reduces HIF-1 $\alpha$  expression [44].

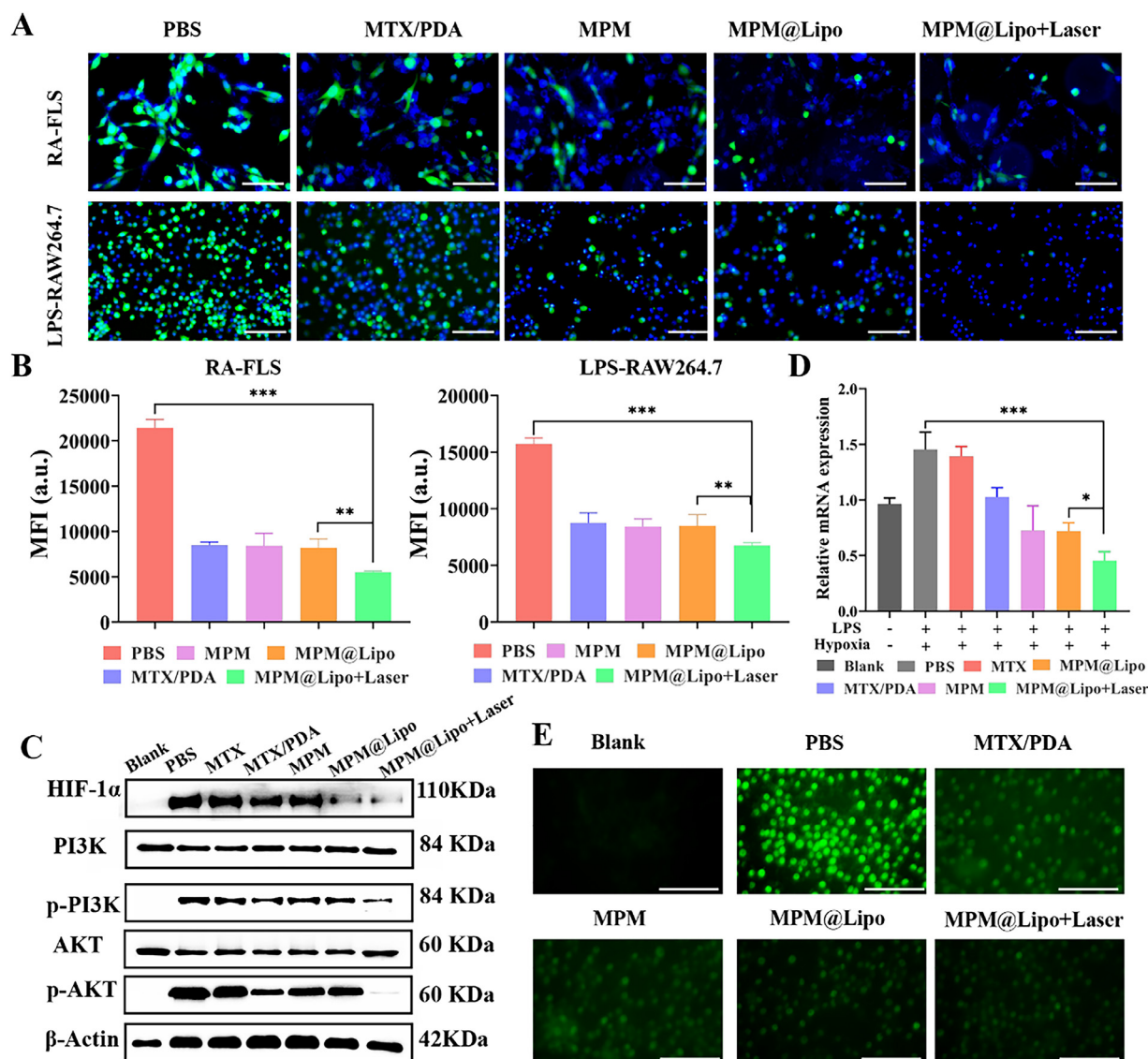


**Fig. 4** – ROS scavenging and regulation of the PI3K-AKT signaling pathway. (A) The intracellular ROS levels in RA-FLSs cells and LPS-activated RAW264.7 cells were observed by fluorescent microscopy, scale bar = 100  $\mu$ m. (B) Intracellular ROS were determined by flow cytometry ( $n = 3$ ), \* $P < 0.05$ , \*\* $P < 0.01$ , \*\*\* $P < 0.001$ . (C) Protein expression of HIF-1 $\alpha$ , PI3K, p-PI3K, AKT and p-AKT in LPS-activated RAW264.7 treated with MTX and MTX-loaded nanoparticles were measured by Western blot. (D) The mRNA expression of HIF-1 $\alpha$  in LPS-activated RAW264.7 cells were detected by RT-PCR ( $n = 3$ ), \* $P < 0.05$ , \*\*\* $P < 0.001$ . (E) Immunofluorescence staining of HIF-1 $\alpha$  (green) in LPS-activated RAW264.7 cells, scale bar = 100  $\mu$ m.

### 3.9. Macrophage phenotype transition

In RA joints, M1 macrophages secrete TNF- $\alpha$ , iNOS, and IL-6 to promote disease progression and exacerbate joint inflammation, while M2 macrophages secrete CD206, IL-10, and Arg-1 (anti-inflammatory factors) to alleviate joint inflammation. iNOS is transcriptionally induced under the action of other proinflammatory cytokines in macrophages to produce excess NO, which is the signature inflammatory factor of M1 macrophages and can cause tissue metabolism hypoxia. Mannose receptor (CD206) is a marker for M2 macrophages, and facilitates the maintenance of intracellular homeostasis. Therefore, the M1/M2 ratio was increased, which may exacerbate the disease process of RA. A potential strategy

for treating RA is to restore the balance between M1 and M2 macrophages.

To investigate the ability of MPM@Lipo to induce macrophage phenotypic transition, immunofluorescence staining was first used to analyze the levels of iNOS and CD206. After treatment with MPM@Lipo and MPM@Lipo+Laser (Fig. 5A), the red fluorescence intensity of the iNOS signal was reduced, while the green fluorescence intensity of CD206 became more pronounced, indicating the effective repolarization of macrophages. The mRNA expression of M1 inflammatory cytokines was significantly ( $P < 0.001$ ) upregulated under the combined stimulation of hypoxia and LPS in the PBS group (Fig. 5B). MPM@Lipo+Laser exhibited stronger downregulation of the mRNA expression

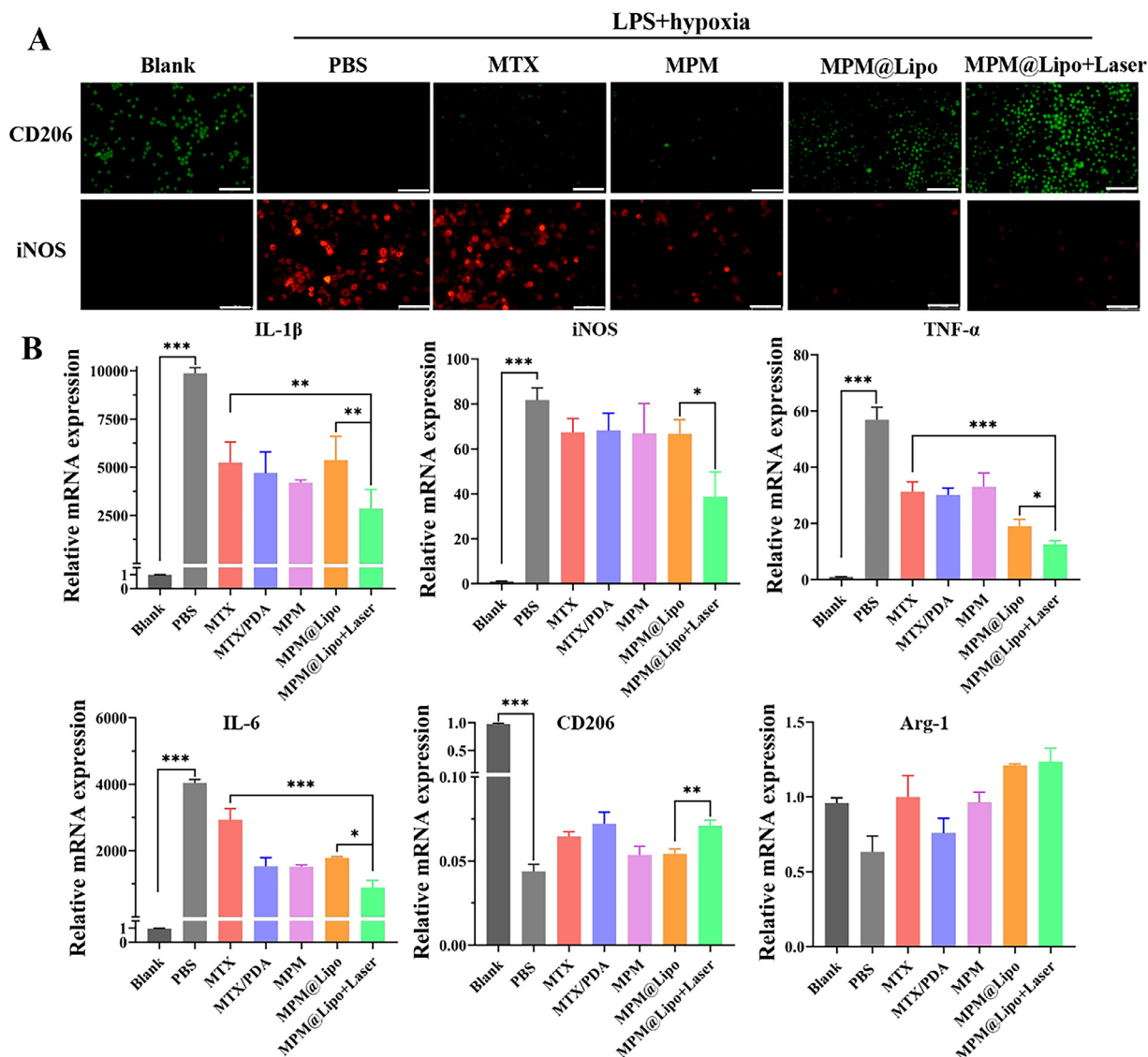


**Fig. 5 – Macrophage phenotype transition. (A) Immunofluorescence staining of iNOS (red) and CD206 (green) in LPS-activated RAW264.7 after various treatments, scale bar = 100  $\mu$ m. (B) The mRNA expression of M1 macrophage markers (IL-1 $\beta$ , IL-6, iNOS and TNF- $\alpha$ ) and M2 macrophage markers (Arg-1 and CD206) in LPS-activated RAW264.7 after various treatments were detected by RT-PCR (n = 3). \*P < 0.05; \*\*P < 0.01; \*\*\*P < 0.001.**

levels of M1 inflammatory cytokines (IL-1 $\beta$ , TNF- $\alpha$ , IL-6 and iNOS) than the other formulations. The mRNA expression levels of Arg-1 and CD206 secreted by anti-inflammatory M2 macrophages were decreased after hypoxia and LPS stimulation. The MPM@Lipo+Laser group had the best effect in upregulating Arg-1 and CD206, which were increased up to 1.97-time and 1.75-time than that of the PBS group, respectively. The results indicated that the MPM@Lipo+Laser group could play an anti-inflammatory role by regulating macrophage phenotype. A decrease in the M1/M2 ratio was observed in each treatment group. Consequently, alleviating hypoxia and ROS scavenging are effective treatments for RA.

### 3.10. Pharmacokinetic study

As depicted in Fig. 6A and Table S2, the concentration of MTX in the MPM@Lipo group declined more slowly than that in

the free MTX group. The area under the plasma concentration curve (AUC<sub>0-t</sub>) of MPM@Lipo (5151.3  $\pm$  776.1 mg/l·h) was 5.46-fold higher than that of MTX (944.3  $\pm$  226.5 mg/l·h). MPM@Lipo showed significantly prolonged blood circulation and facilitated the accumulation of nanoparticles in inflamed joints.

### 3.11. In vivo targeting efficiency

Near-infrared fluorescence imaging was used to evaluate the *in vivo* targeting efficiency of intravenously administered DIR and DIR/PM@Lipo (Fig. 6B). Strong fluorescence signals accumulated in the hind paw of rats 1 h after DIR/PM@Lipo injection into the tail vein of rats, which reached a maximum at 24 h. Compared with free DIR, DIR/PM@Lipo exhibited stronger fluorescence signals in inflamed joints at various time points, suggesting that DIR/PM@Lipo could effectively

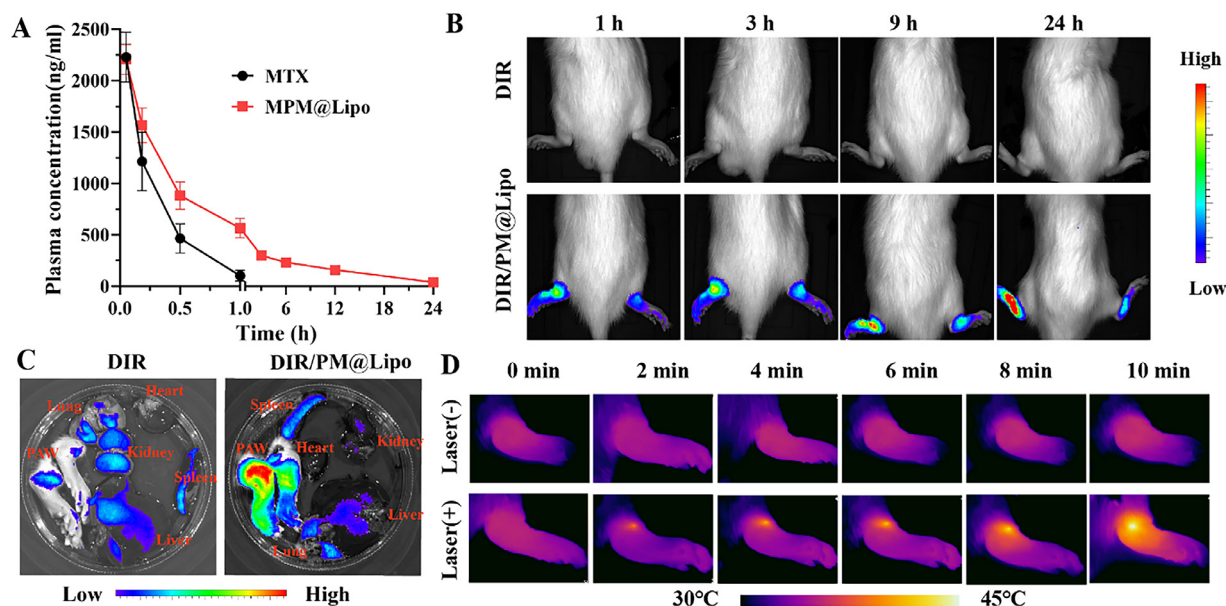


**Fig. 6** – Pharmacokinetics and biodistribution study. (A) The concentration versus time curve of MTX after intravenous injection of MTX and MPM@Lipo in rats, ( $n = 6$ ). (B) Accumulation of DIR and DIR/PM@Lipo in the paws of AIA rat was monitored by *in vivo* fluorescence image system. (C) *Ex vivo* imaging of the organs and paws at 24 h after intravenous injection. (D) Photothermal images of the ankle of AIA rats in MPM@Lipo group under laser irritation.

accumulate in the joint site with improved targeting. Furthermore, *ex vivo* imaging from DIR/PM@Lipo-treated rats showed that inflammatory paws had marked fluorescence (Fig. 6C).

### 3.12. Photothermal effect of MPM@Lipo *in vivo*

As shown in Fig. 6D, under local irradiation with the NIR laser ( $1.5 \text{ W/cm}^2$ , 10 min), the temperature of the inflammatory joint in the MPM@Lipo+Laser group rapidly increased to approximately  $44 \text{ }^\circ\text{C}$ , while the temperature in the MPM@Lipo without laser group had almost no significant change. The results showed that MPM@Lipo had superior photothermal properties *in vivo*.

### 3.13. *In vivo* therapeutic effect of MPM@Lipo on RA

#### 3.13.1. Evaluation of arthritis scores and paw thickness

The protocol for AIA rat treatment is shown in Fig. 7A. As the disease progressed, the arthritis scores of the saline-treated group rats continued to increase (Fig. 7B). After treatment with free MTX, MPM, MPM@Lipo and MPM@Lipo+Laser, the arthritis scores of AIA rats began to slowly decrease. Arthritis scores showed the greatest decrease in the MPM@Lipo+Laser group compared with the other treatment groups. On Day 33, the arthritis scores in each group were  $3.875 \pm 0.35$ ,  $3.125 \pm 0.99$ ,  $3.125 \pm 1.13$ ,  $2.857 \pm 0.69$  and  $1.875 \pm 0.99$ , respectively. The changes in swelling rates were quantified by examining joint thickness and paw volume (Fig. 7C and D), and their trends were consistent with the arthritis scores in each group. With the extension of treatment time, paw thickness and paw volume decreased to a certain extent.

After treatment, the paw thickness in the saline treatment group reached  $10.24 \pm 1.30 \text{ mm}$ , and those in the MTX, MPM, MPM@Lipo and MPM@Lipo+Laser treatment groups decreased to  $8.04 \pm 1.42$ ,  $6.24 \pm 0.27$ ,  $6.29 \pm 0.35$ , and  $5.02 \pm 0.47 \text{ mm}$ , respectively. Paw volume showed the same trend as paw thickness (Fig. S12). There was a significant decrease in paw volume in the MTX and MTX nanoparticle groups compared with the saline group. On the 33rd d after immunization, the hind limbs of rats treated with MTX and MTX-loaded nanoparticles were photographed and shown in Fig. 7E. Multiple joint swelling and severe deformity of the whole paw were observed in the saline group, while these symptoms were significantly alleviated in the MTX, MPM, MPM@Lipo and MPM@Lipo+Laser groups. As expected, there was only mild swelling and limited erythema in the MPM@Lipo and MPM@Lipo+Laser groups. In summary, MPM@Lipo+Laser exhibited reduced inflammation scores and paw swelling and a better treatment effect.

#### 3.13.2. Cytokine determination

Both of TNF- $\alpha$  and IL-6 are representative proinflammatory factors in AIA joints. Fig. 7F and G showed that the content of TNF- $\alpha$  in the saline group was  $18.98 \text{ pg/ml}$ , and after MTX, MPM, MPM@Lipo and MPM@Lipo+Laser treatment, the concentration of TNF- $\alpha$  decreased to  $11.76$ ,  $9.29$ ,  $9.08$  and  $6.15 \text{ pg/ml}$ , respectively. The change trend of the IL-6 concentration was consistent with that of TNF- $\alpha$ . Notably, the MPM@Lipo+Laser group showed the best inhibition of inflammatory factors. The results indicated that MPM@Lipo could generate heat rapidly and kill inflammatory cells under laser irradiation, and was an excellent photothermal agent for RA treatment.

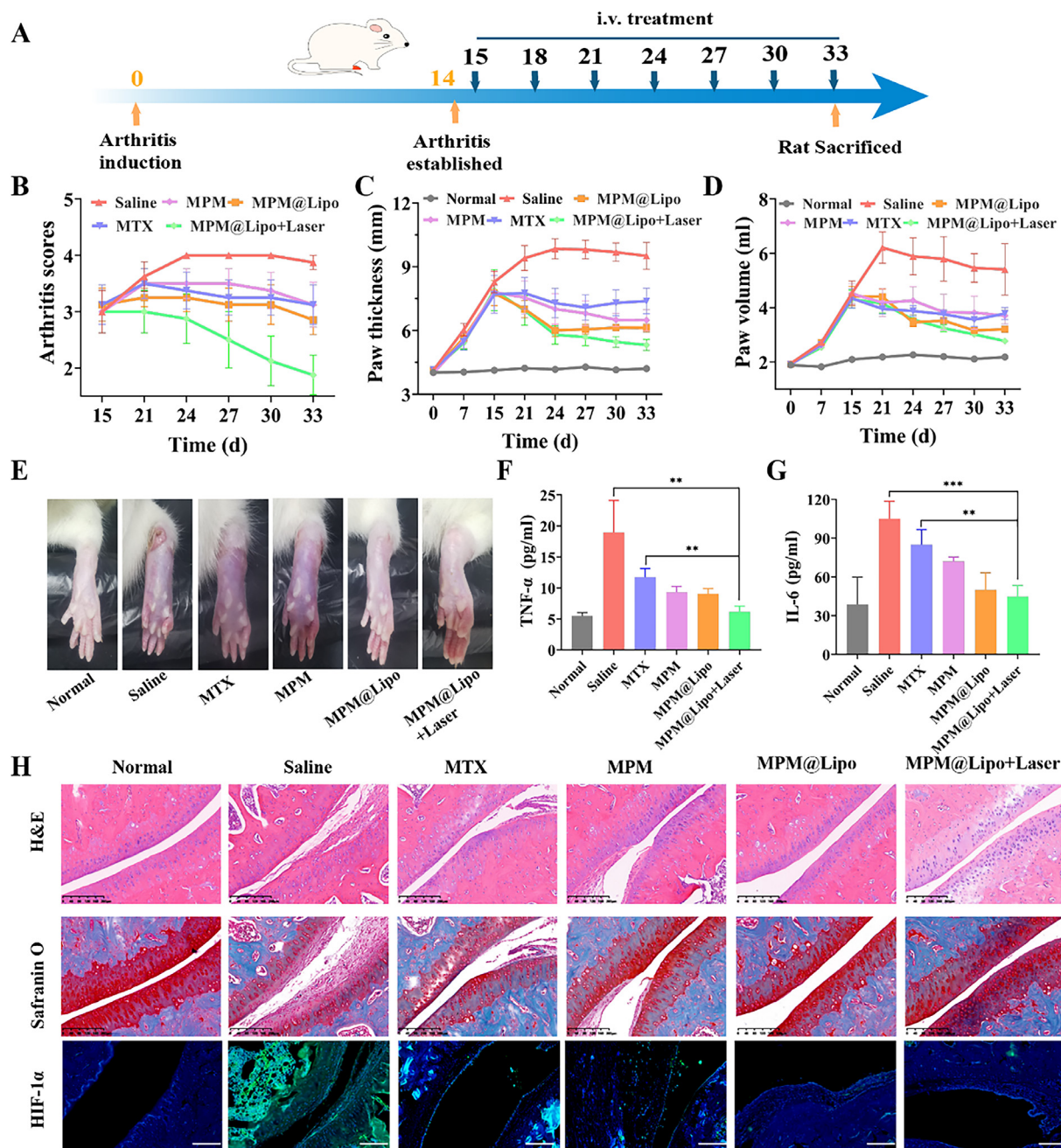


**Fig. 7 – In vivo therapeutic efficacy evaluation. (A) AIA model establishment and treatment protocol in rats. (B) Arthritis scores in different groups during 18-d treatment ( $n = 6$ , mean  $\pm$  SEM). (C) Right paw swelling thickness and (D) paw volume change curves in AIA rats ( $n = 6$ , mean  $\pm$  SEM). (E) Representative photograph of right hind limbs after treatment. The levels of (F) TNF- $\alpha$  and (G) IL-6 in different groups were measured by ELISA ( $n = 6$ ), \*\* $P < 0.01$ , \*\*\* $P < 0.001$ . (H) Histopathology evaluation of the ankle joints was identified using H&E, Safranin-O Fast green staining and HIF-1 $\alpha$  immunofluorescent staining, scale bar=200  $\mu$ m.**

### 3.13.3. Histological analysis

The therapeutic effect of MPM@Lipo on RA was analyzed by pathological staining (Fig. 7H). Unclear bone boundaries, joint destruction, and inflammatory cell infiltration were observed in saline-treated AIA rats. The pathological state of AIA was significantly improved after treatment with MTX and MTX-loaded nanoparticles, especially in the MPM@Lipo+Laser

group. The bone boundary of MPM@Lipo+Laser was clear, the cartilage was smooth and intact, and no inflammatory cell infiltration was observed.

Safranin-O/fast green staining can be used to evaluate the loss of cartilage proteoglycans and the degree of cartilage damage. The articular cartilage in the normal group was smooth and intact with bright red staining. The articular

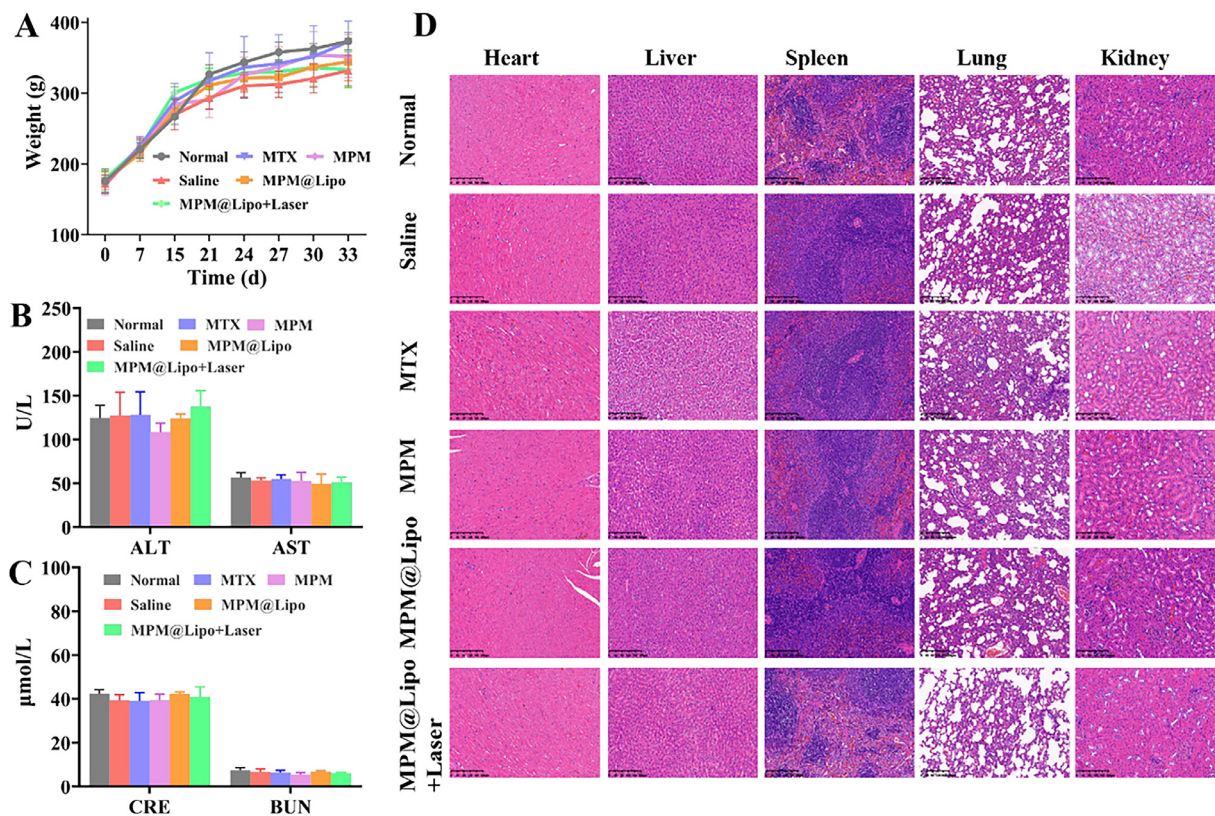


**Fig. 8 – Safety evaluation. (A) Change of body weight in different groups ( $n = 6$ ). (B) Hepatotoxicity and (C) nephrotoxicity were evaluated by measuring serum levels of ALT, AST, BUN and CRE ( $n = 6$ ). (D) H&E staining of heart, liver, spleen, lung and kidney after treatments, scale bar = 200  $\mu\text{m}$ .**

cartilage layer in the saline group was destroyed, and the safranin O staining was weak, indicating the loss of large amounts of proteoglycans. The articular cartilage in the MPM@Lipo+Laser group was smooth and bright red. Immunofluorescence staining (Fig. 7H and S13) showed that HIF-1 $\alpha$  was highly expressed in the saline group. After treatment with MPM, MPM@Lipo and MPM@Lipo+Laser, the expression was significantly reduced, especially in the MPM@Lipo and MPM@Lipo+Laser groups. The application of NIR irradiation in RA is expected to not only improve the efficacy of nanoparticles but also relieve the related symptoms of inflammatory arthritis. Under laser irradiation, MTX and oxygen were released from MPM@Lipo in a burst manner, allowing MTX and oxygen to rapidly reach an effective concentration to exert therapeutic effects. In conclusion, *in vivo* experiments showed that the MPM@Lipo combination PTT exhibited synergistic anti-inflammatory effects, inhibited RA disease progression, reduced cartilage tissue damage, and did not cause organ toxicity.

### 3.14. Safety evaluation

Changes in body weight are also reliable indicators of diseased conditions. During the treatment period, the average body weight of rats in each group increased gradually, and no obvious changes were found among the treatment groups (Fig. 8A). The blood biochemical results showed that after

injection of MTX or MTX-loaded nanoparticles into the tail vein, the detected levels of ALT and AST remained stable and within the normal range for both the treatment group and controls (Fig. 8B and C), indicating no hepatotoxicity or nephrotoxicity. The H&E sections of main organs (Fig. 8D) were all similar among the treatment groups and normal group, indicating good *in vivo* safety. The results strongly suggest that this formulation has good biological safety and is an effective nanodelivery system for targeted RA treatment.

## 4. Conclusion

In this study, we successfully constructed the nanocarrier MPM@Lipo with high photothermal conversion capability for PTT, MTX delivery, ROS scavenging and oxygen generation. MPM@Lipo combined with laser irradiation can effectively induce inflammatory cell death, scavenge excess ROS, reprogram M1/M2 macrophages, and suppress the generation of proinflammatory cytokines. The oxygen produced significantly ameliorated the hypoxic microenvironment and downregulated the expression of HIF-1 $\alpha$ . *In vivo* experiments confirmed that MPM@Lipo targeted inflamed joints and accumulated efficiently, which improved the safety and therapeutic effect of MTX. The multifunctional MPM@Lipo showed good biocompatibility and excellent anti-inflammatory activity and photothermal effects under NIR

irradiation, which is beneficial for RA therapy. In summary, this study reveals the potential of MPM@Lipo and provides new ideas for designing PDA-based anti-inflammatory nanoplatforams for RA treatment.

### Conflicts of interest

The authors report no conflicts of interest. The authors alone are responsible for the content and writing of this article.

### Supplementary materials

Supplementary material associated with this article can be found, in the online version, at [doi:10.1016/j.ajps.2024.100885](https://doi.org/10.1016/j.ajps.2024.100885).

### REFERENCES

- Wang S, Chen R, Yu Q, Huang W, Lai P, Tang J, et al. Near-infrared plasmon-boosted heat/oxygen enrichment for reversing rheumatoid arthritis with metal/semiconductor composites. *ACS Appl Mater Interfaces* 2020;12:45796–806.
- Zhang G, Sun G, Guan H, Li M, Liu Y, Tian B, et al. Naringenin nanocrystals for improving anti-rheumatoid arthritis activity. *Asian J Pharm Sci* 2021;16:816–25.
- Li Y, Liang Q, Zhou L, Cao Y, Yang J, Li J, et al. An ROS-responsive artesunate prodrug nanosystem co-delivers dexamethasone for rheumatoid arthritis treatment through the HIF-1 $\alpha$ /NF- $\kappa$ B cascade regulation of ROS scavenging and macrophage repolarization. *Acta Biomater* 2022;152:406–24.
- Tian J, Chen T, Huang B, Liu Y, Wang C, Cui Z, et al. Inflammation specific environment activated methotrexate-loaded nanomedicine to treat rheumatoid arthritis by immune environment reconstruction. *Acta Biomater* 2023;157:367–80.
- Guo T, Kang X, Ren S, Ouyang X, Chang M. Construction of a nano-controlled release methotrexate delivery system for the treatment of rheumatoid arthritis by local percutaneous administration. *Nanomaterials* 2021;11:2812.
- Wang Q, Sun X. Recent advances in nanomedicines for the treatment of rheumatoid arthritis. *Biomater Sci* 2017;5:1407–20.
- Chen X, Zhu X, Xu T, Xu M, Wen Y, Liu Y, et al. Targeted hexagonal Pd nanosheet combination therapy for rheumatoid arthritis via the photothermal controlled release of MTX. *J Mater Chem B* 2019;7:112–22.
- Yang N, Li M, Wu L, Song Y, Yu S, Wan Y, et al. Peptide-anchored neutrophil membrane-coated biomimetic nanodrug for targeted treatment of rheumatoid arthritis. *J Nanobiotechnology* 2023;21.
- Feng C, Pan L, Qin X, Li D, Chen T, Lin Z, et al. Inflammation-homing “living drug depot” for efficient arthritis treatment. *Acta Biomater* 2022;150:324–36.
- Vanniasinghe AS, Manolios N, Schibeci S, Lakhiani C, Kamali-Sarvestani E, Sharma R, et al. Targeting fibroblast-like synovial cells at sites of inflammation with peptide targeted liposomes results in inhibition of experimental arthritis. *Clin Immunol* 2014;151:43–54.
- Yang Y, Luo S, Peng X, Zhao T, He Q, Wu M, et al. An intra-articular injectable phospholipids-based gel for the treatment of rheumatoid arthritis. *Asian J Pharm Sci* 2023;18:100777.
- Kim J, Kim HY, Song SY, Go S-h, Sohn HS, Baik S, et al. Synergistic oxygen generation and reactive oxygen species scavenging by manganese ferrite/ceria co-decorated nanoparticles for rheumatoid arthritis treatment. *ACS Nano* 2019;13:3206–17.
- Liu X, Guo R, Huo S, Chen H, Song Q, Jiang G, et al. CaP-based anti-inflammatory HIF-1 $\alpha$  siRNA-encapsulating nanoparticle for rheumatoid arthritis therapy. *J Control Release* 2022;343:314–25.
- Ma Q, Bai J, Xu J, Dai H, Fan Q, Fei Z, et al. Reshaping the inflammatory environment in rheumatoid arthritis joints by targeting delivery of berberine with platelet-derived extracellular vesicles. *Adv Nanobiomed Res* 2021;1:2100071.
- Lu Y, Li L, Lin Z, Wang L, Lin L, Li M, et al. A new treatment modality for rheumatoid arthritis: combined photothermal and photodynamic therapy using Cu<sub>7</sub>2S<sub>4</sub> nanoparticles. *Adv Healthc Mater* 2018;7:1800013.
- Huang R, Zhang C, Bu Y, Li Z, Zheng X, Qiu S, et al. A multifunctional nano-therapeutic platform based on octahedral yolk-shell Au NR@CuS: photothermal/photodynamic and targeted drug delivery tri-combined therapy for rheumatoid arthritis. *Biomaterials* 2021;277:121088.
- Gadeval A, Chaudhari S, Bollampally SP, Polaka S, Kalyane D, Sengupta P, et al. Integrated nanomaterials for non-invasive photothermal therapy of rheumatoid arthritis. *Drug Discov Today* 2021;26:2315–28.
- Lu J, Cai L, Dai Y, Liu Y, Zuo F, Ni C, et al. Polydopamine-based nanoparticles for photothermal therapy/chemotherapy and their synergistic therapy with autophagy inhibitor to promote antitumor treatment. *Chem Rec* 2021;21:781–96.
- Yu H, Fan J, Shehla N, Qiu Y, Lin Y, Wang Z, et al. Biomimetic hybrid membrane-coated xuetongsu assisted with laser irradiation for efficient rheumatoid arthritis therapy. *ACS Nano* 2021;16:502–21.
- Wei Y, Nie Y, Han Z, Huang H, Liao X, Wang X, et al. Au@polydopamine nanoparticles/tocilizumab composite as efficient scavengers of oxygen free radicals for improving the treatment of rheumatoid arthritis. *Mater Sci Eng: C* 2021;118:111434.
- Liu S, Zhang C, Zhou Y, Zhang F, Duan X, Liu Y, et al. MRI-visible mesoporous polydopamine nanoparticles with enhanced antioxidant capacity for osteoarthritis therapy. *Biomaterials* 2023;295:122030.
- Zhao H, Zeng Z, Liu L, Chen J, Zhou H, Huang L, et al. Polydopamine nanoparticles for the treatment of acute inflammation-induced injury. *Nanoscale* 2018;10:6981–91.
- Bao X, Zhao J, Sun J, Hu M, Yang X. Polydopamine nanoparticles as efficient scavengers for reactive oxygen species in periodontal disease. *ACS Nano* 2018;12:8882–92.
- Huang X, He D, Pan Z, Luo G, Deng J. Reactive-oxygen-species-scavenging nanomaterials for resolving inflammation. *Materials Today Bio* 2021;11:100124.
- Li C, Zhao Z, Luo Y, Ning T, Liu P, Chen Q, et al. Macrophage-disguised manganese dioxide nanoparticles for neuroprotection by reducing oxidative stress and modulating inflammatory microenvironment in acute ischemic stroke. *Adv Sci* 2021;8:2101526.
- Wu C, Cheng J, Li W, Yang L, Dong H, Zhang X. Programmable polymeric microneedles for combined chemotherapy and antioxidative treatment of rheumatoid arthritis. *ACS Appl Mater Interfaces* 2021;13:55559–68.
- Liu Y, Xu J, Liu L, Tan J, Gao L, Wang J, et al. Amorphous manganese dioxide coated polydopamine nanoparticles for acid-sensitive magnetic resonance imaging-guided tumor photothermal therapy. *J Biomed Nanotechnol* 2019;15:1771–80.
- Zhang H, Tang W-L, Kheirrolomoom A, Fite BZ, Wu B, Lau K, et al. Development of thermosensitive resiquimod-loaded liposomes for enhanced cancer immunotherapy. *J. Control. Release* 2021;330:1080–94.

- [29] Jose A, Ninave KM, Karnam S, Venuganti VVK. Temperature-sensitive liposomes for co-delivery of tamoxifen and imatinib for synergistic breast cancer treatment. *J Liposome Res* 2018;29:153–62.
- [30] Zhao J, Zhao M, Yu C, Zhang X, Liu J, Cheng X, et al. Multifunctional folate receptor-targeting and pH-responsive nanocarriers loaded with methotrexate for treatment of rheumatoid arthritis. *Int J Nanomedicine* 2017;12:6735–46.
- [31] Daraghme DN, Moghaddami M, Bobrovskaya L, Proudman SM, Wiese MD. Quantitation of methotrexate polyglutamates in human whole blood, erythrocytes and leukocytes collected via venepuncture and volumetric absorptive micro-sampling: a green LC-MS/MS-based method. *Anal. Bioanal. Chem.* 2022;414:6029–46.
- [32] Hu Q, Fu X, Dong Y, Ma J, Hua J, Li J, et al. D-optimal design and development of a koumine-loaded microemulsion for rheumatoid arthritis treatment: *in vivo* and *in vitro* evaluation. *Int J Nanomedicine* 2023;18:2973–88.
- [33] Chen X, Zhu X, Ma L, Lin A, Gong Y, Yuan G, et al. A core-shell structure QRu-PLGA-RES-DS NP nanocomposite with photothermal response-induced M2 macrophage polarization for rheumatoid arthritis therapy. *Nanoscale* 2019;11:18209–23.
- [34] Xi Y, Xie X, Peng Y, Liu P, Ding J, Zhou W. DNAzyme-adsorbed polydopamine@MnO<sub>2</sub> core-shell nanocomposites for enhanced photothermal therapy via the self-activated suppression of heat shock protein 70. *Nanoscale* 2021;13:5125–35.
- [35] Nygaard G, Firestein GS. Restoring synovial homeostasis in rheumatoid arthritis by targeting fibroblast-like synoviocytes. *Nat Rev Rheumatol* 2020;16:316–33.
- [36] Li B, Liu F, Ye J, Cai X, Qian R, Zhang K, et al. Regulation of macrophage polarization through periodic photo-thermal treatment to facilitate osteogenesis. *Small* 2022;18:2202691.
- [37] Li Y, Zhai Y, Liu W, Zhang K, Liu J, Shi J, et al. Ultrasmall nanostructured drug based pH-sensitive liposome for effective treatment of drug-resistant tumor. *J Nanobiotechnology* 2019;17.
- [38] Zhang L, Qin Z, Sun H, Chen X, Dong J, Shen S, et al. Nanoenzyme engineered neutrophil-derived exosomes attenuate joint injury in advanced rheumatoid arthritis via regulating inflammatory environment. *Bioact Mater* 2022;18:1–14.
- [39] Zheng C, Wu A, Zhai X, Ji H, Chen Z, Chen X, et al. The cellular immunotherapy of integrated photothermal anti-oxidation Pd–Se nanoparticles in inhibition of the macrophage inflammatory response in rheumatoid arthritis. *Acta Pharm Sin B* 2021;11:1993–2003.
- [40] Li G, Zhang Y, Liu D, Qian Y, Zhang H, Guo S, et al. PI3 kinase/Akt/HIF-1 $\alpha$  pathway is associated with hypoxia-induced epithelial-mesenchymal transition in fibroblast-like synoviocytes of rheumatoid arthritis. *Mol. Cell. Biochem.* 2012;372:221–31.
- [41] Vergadi E, Ieronymaki E, Lyroni K, Vaporidi K, Tsatsanis C. Akt signaling pathway in macrophage activation and M1/M2 polarization. *J Immunol* 2017;198:1006–14.
- [42] Ao L, Gao H, Jia L, Liu S, Guo J, Liu B, et al. Matrine inhibits synovial angiogenesis in collagen-induced arthritis rats by regulating HIF-VEGF-Ang and inhibiting the PI3K/Akt signaling pathway. *Mol Immunol* 2022;141:13–20.
- [43] Lin Y, Zheng F, Xiong B, Chen Z, Chen S, Fang C, et al. Koumine alleviates rheumatoid arthritis by regulating macrophage polarization. *J Ethnopharmacol* 2023;311:116474.
- [44] Chen M, Lu Q, Chen Y, Hou Y, Zou Y-M, Zhou Q, et al. NIR-PTT/ROS-scavenging/oxygen-enriched synergetic therapy for rheumatoid arthritis by a pH-responsive hybrid CeO<sub>2</sub>-ZIF-8 coated with polydopamine. *ACS Biomater Sci Eng* 2022;8:3361–76.